THE JOURNAL OF PHYSICAL CHEMISTRY A
A JOURNAL OF THE AMERICAN CHEMICAL SOCIETY

pubs.acs.org/JPCA Article

Switching between Proton Vacancy and Excess Proton Transfer Pathways in the Reaction between 7-Hydroxyquinoline and Formate

Marius-Andrei Codescu, Moritz Weiß, Martin Brehm, Oleg Kornilov, Daniel Sebastiani,* and Erik T. J. Nibbering*

Cite This: J. Phys. Chem. A 2021, 125, 1845−1859 Read Online

ACCESS | Metrics & More | Article Recommendations | Supporting Information

ABSTRACT: Bifunctional or amphoteric photoacids simultaneously present donor (acidic) and acceptor (basic) properties making them useful tools to analyze proton transfer reactions. In protic solvents, the proton exchange between the acid and the base is controlled by the acidity or basicity strength and typically occurs on two different pathways known as protolysis and hydrolysis. We report here how the addition of a formate base will alter the relative importance of the possible reaction pathways of the bifunctional photoacid 7-hydroxyquinoline (7HQ), which has been recently understood to predominantly involve a hydroxide/methoxide transport mechanism between the basic proton-accepting quinoline nitrogen site toward the proton-donating OH group with a time constant of 360 ps in deuterated methanol (CD_3OD). We follow the reaction dynamics by probing the IR-active marker modes of the different charged forms of photoexcited 7HQ, and of formic acid (HCOOD) in CD_3OD solution. A comparison of the transient IR spectra as a function of formate concentration, and classical molecular dynamics simulations enables us to identify distinct contributions of "tight" (meaning "contact") and "loose" (i.e., "solvent-separated") 7HQ−formate reaction pairs in our data. Our results suggest that depending on the orientation of the OH group with respect to the quinoline aromatic ring system, the presence of the formate molecule in a proton relay pathway facilitates a net proton transfer from the proton-donating OH group of 7HQ-N* via the methanol/formate bridge toward the quinoline N site.

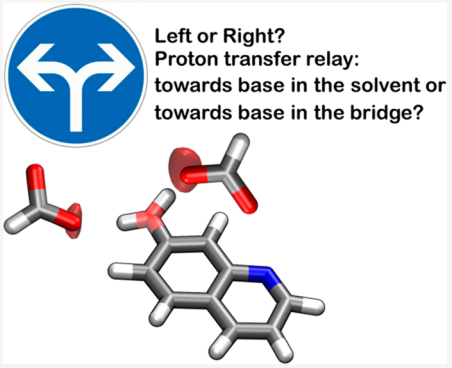

1. INTRODUCTION

Proton transport is at the heart of many energy conversion processes ranging from light harvesting[1−5] to hydrogen fuel cells.[6−8] The underlying microscopic mechanisms for proton transport have been intensively studied in the last decades.[9−17] Here the elementary steps of proton transfer, both in the bulk solvent and from proton-donating acids to the solvent and from the solvent to proton-accepting bases have been a major focus in experimental and theoretical research efforts. From ab initio molecular dynamics (AIMD) simulations it has become clear that the transfer of an excess proton involves ultrafast hydrogen bond rearrangements of, in particular, the first hydration shell water molecules around a hydrated proton complex, strongly governing the time scales for excess proton transport in bulk water, known as the von Grotthuss mechanism.[9−11,13,18,19] In a similar fashion hydroxide transport, which involves the translocation of a proton vacancy ("proton hole"), is determined by consecutive ultrafast hydrogen bond rearrangements, albeit significant differences in the nature and number of hydration shell hydrogen bond interactions have been noted.[12,15,17,20] In contrast to proton transport in bulk water, solvent mediated proton transport between acids and bases enables one to explore the transport mechanisms with well-defined start and end points.[12,21,22] With such molecular systems questions on the directionality of proton transport pathways can be better explored.

Photoacids and photobases, molecular systems that respectively exhibit a profound increase in acidity or basicity,[23,24] are ideal molecular tools to study proton transport dynamics on ultrafast time scales using short pulse laser systems.[25,26] Proton dissociation to or proton abstraction from water and alcohol solvents[27−34] and photoacid−base neutralization reactions[35−40] have been investigated with picosecond time-correlated single photon counting, femtosecond UV−vis and UV−IR pump−probe techniques. A special class are so-called bifunctional photoacids and photobases,[41−46] where proton-donating and -accepting sites are part of the same molecular system, with a well-defined number of solvent molecules constituting the proton transport pathway between donating and accepting sites. In a recent study[45,47,48] we have used 7-hydroxyquinoline (7HQ; see Figure 1a), which is both

Received: November 11, 2020
Revised: February 22, 2021
Published: March 2, 2021

https://dx.doi.org/10.1021/acs.jpca.0c10191
J. Phys. Chem. A 2021, 125, 1845−1859

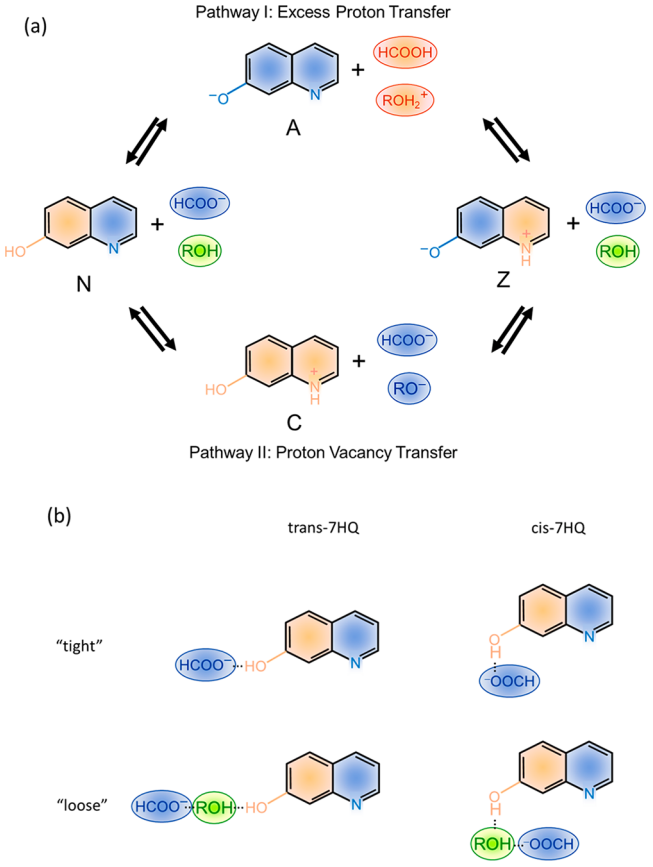

Figure 1. (a) Proton transfer pathways of 7HQ in methanol with formate anion as additional reaction partner. Formate only plays a direct role in the acid–base chemistry of 7HQ, acting as an alternative carrier for proton transport in the excess proton transfer pathway I, whereas the proton vacancy transfer pathway II will predominantly not involve a direct participation of formate anions. (b) Examples of "tight" contact and "loose" solvent-separated acid–base reaction pairs of *trans*-7HQ or *cis*-7HQ with formate anion.

a photoacid and a photobase through its hydroxyl proton-donating and quinoline nitrogen proton-accepting functionalities, to explore the proton transport pathways in water/methanol mixtures. We have found that proton abstraction by the quinoline nitrogen is the rate-determining step (N* → C*), followed by hydroxide/methoxide transfer toward the hydroxyl proton-donating site, completing the proton transport (through the C* → Z* step). Hence proton vacancy transport prevails in the scheme of possible proton transport pathways, a mere consequence of proton abstraction from the solvent by the quinoline nitrogen being faster than proton donation to the solvent by the hydroxyl group, as the subsequent proton transfer steps through the solvent bridge are much faster and cannot affect the overall outcome of the proton transport dynamics.

The objective of the current report is to investigate whether the addition of a base would accelerate the proton donation from the hydroxyl group of 7HQ (leading to the N* → A* step) in such a way that a quantitative steering of the proton transport dynamics from proton vacancy to excess proton transfer is possible, and with this a switch is made from the hydrolysis/methanolysis pathway II to the protolysis pathway I as the dominant proton transport mechanism. For this, we build on previous achievements obtained on and conclusions drawn from photoacid–carboxylate neutralization studies.[35−40] We investigate here the proton transfer dynamics of 7HQ reacting with cesium formate in methanol by use of femtosecond UV–IR pump–probe spectroscopy. Previous studies have estimated the change in acidity for the hydroxyl group of 7HQ upon photoexcitation of 7HQ-N → 7HQ-N* to be $\Delta pK_a = pK_a^* - pK_a = 0.4-8.67 = -8.3$ in H_2O solution.[41,42,47] We have estimated this change to $\Delta pK_a = pK_a^* - pK_a = 4.1-13.02 = -8.9$ in CH_3OH solution, and $\Delta pK_a = pK_a^* - pK_a = 4.6-13.5 = -8.9$ in CD_3OD solution, respectively (see also the Supporting Information).[48] Realizing that the acidity of formic acid (HCOOH/HCOOD) is pK_a = 3.75 in H_2O solution, and 8.77 in CH_3OH (9.3 in CD_3OD), a net proton/deuteron transfer between the hydroxyl group of 7HQ and formate is anticipated in a similar fashion as for HPTS-acetate neutralization experiments. Using (sub)molar concentration of formate, we show that a major fraction of photoexcited 7HQ indeed follows the excess proton transfer route, albeit with a smaller amount of formic acid being able to further mediate the proton transfer enabling the 7HQ A* → Z* conversion. To assess possible spatial distribution functions of the ions around 7HQ we present results from classical molecular dynamics simulations. A preferential location of formate near the OH group of 7HQ implies the observed ultrafast proton transfer dynamics of 7HQ occurs predominantly toward formate. Relative orientations of the O–H bond vector with respect to the quinoline aromatic ring system determine subsequent proton transfer steps (Figure 1b). We explore the possibilities of subsequent proton transfer into the solvent or toward the quinoline N site.

2. METHODS

2.1. Materials. 7-Hydroxyquinoline (7HQ, 99% purity, ACROS Organics) and cesium formate ($HCOO^-Cs^+$, 98% purity, Alfa Aesar) were used without further purification. Solutions of 7HQ and cesium formate dissolved in deuterated methanol (CD_3OD, >99.8 purity, Deutero GmbH) were prepared for our studies.

2.2. Steady-State Absorption and Emission Measurements. We recorded UV–vis absorption spectra with a resolution of 1 nm by a PerkinElmer LAMBDA 950 UV/vis spectrophotometer and IR absorption spectra with a resolution of 2 cm^{-1} by a Bruker Vertex 80v FT-IR spectrometer. We measured fluorescence emission spectra with a Horiba Scientific Fluorolog-3 FL-1039/40 spectrofluorometer. We set the concentration of 7HQ to a value of 50 mM in methanol for both linear UV–vis and IR absorption measurements. We used a Harrick Cell equipped with a 56 μm thick Teflon spacer to measure our liquid solutions. For the fluorescence emission measurements we used a 10 mm quartz cuvette, for which we varied the concentrations of 7HQ to values as low as 1 mM to suppress reabsorption of the fluorescence emission. We selected $HCOO^-Cs^+$ as the proton acceptor because of its sufficient basicity and high solubility of up to 8.5 mol/L in methanol at room temperature.

2.3. Femtosecond UV/IR Pump–Probe Spectroscopic Measurements. We used a Spectra Physics Ti:sapphire amplified laser system consisting of a Tsunami Ti:sapphire oscillator and a Spitfire Pro regenerative and booster amplifier stages to generate compressed laser pulses with 5 mJ energy at a repetition rate of 1 kHz, centered at 800 nm with a duration of about 55 fs. We directed the compressed pulses through by a beam splitter, after which we used 2.4 mJ of pulse pump

https://dx.doi.org/10.1021/acs.jpca.0c10191
J. Phys. Chem. A 2021, 125, 1845−1859

energy as input in a commercial optical parametric amplifier (TOPAS from Light Conversion) to generate the UV pump pulses and 1.3 mJ of pulse pump energy as input into a double-pass home-built optical parametric amplifier generating the tunable mid-IR probe pulses. The TOPAS enabled UV pulse generation centered at a 330 nm carrier wavelength, with a 55 fs pulse duration through sum-frequency generation by taking the fourth harmonic of the signal pulse created in a nonlinear 4 mm thick barium borate (BBO) crystal. The mid-IR pulses, with 150−200 fs duration, were tuned to central wavelengths ranging from 5.7 to 7.5 μm by a difference frequency generation GaSe crystal of 1 mm thickness. We measured the beam spatial profiles of both UV-pump and mid-IR-probe beams by the knife-edge technique, to ascertain that the diameter of the UV beam (around 170−200 μm in the focal point of mid-IR pulse) was larger than mid-IR beam diameter (around 120−150 μm in the focal point) so we homogeneously excited our samples. In order to avoid multiphoton and cross-phase modulation signal contributions from the solvent and/or from the sample cell windows, we also stretched the UV pulses in time, from 55 fs to around 150−200 fs, by a 3 cm long fused silica cell filled with water placed in the pulse beam pathway. We arranged for mid-IR probe and reference beams by sending the mid-IR pulses through a ZnSe wedge (with a 0.5° angle between front and back sides). After the spatial overlap of the pump and probe pulses was established in the sample, the time delay was then varied by a delay stage (Physik Instrumente 12 in. scanning range, 0.4 μm shortest step range) controlled by Lab View software. By spectrally dispersing the IR beams in a Jobin Yvon polychromator, we recorded absorbance changes in our samples with a double-array (2 × 64 pixels) HgCdTe infrared detector (IR Associates). We determined the time resolution of the pump−probe experiments by means of cross-correlation measurements in a thin ZnSe window to be around 350−400 fs. We refer to further details of our experimental setup reported elsewhere.[40,47]

We examine here the ultrafast proton transfer dynamics of the molecules. With the UV-pump mid-IR-probe geometry, our femtosecond lasers provided snapshots of the time-resolved kinetic profiles. We photoexcited 7HQ with a 150−200 fs long pump pulse tuned at 330 nm, i.e., the maximum absorption peak of the $S_0 \rightarrow S_1$ transition of 7HQ in its neutral tautomer 7HQ-N. After electronic excitation by the UV-pump pulse, we followed the progress of 7HQ−formate reaction kinetics by following the absorbance changes of IR-active marker modes of the different charged states of photoexcited 7HQ and of deuterated formic acid HCOOD with a mid-IR probe pulse. Since the rotational diffusion motions occur on time scales of hundreds of picoseconds, similar to those of the proton transfer dynamics in this study, we performed the measurements under magic-angle geometry between our linearly polarized pump and probe pulses. We used a zero-order half wave-plate to rotate the polarization of the pump pulse to 54.7° with respect to the probe pulse.

To prevent sample damage, we used a peristaltic pump to guarantee a continuous replenishment of the solutions with an average speed of 0.9 mL/second through the Harrick Cell consisting of two CaF_2 windows with a diameter of 25.4 mm, 1 mm thickness each and, separated by a Teflon spacer with 56 μm thickness. We checked for any sample changes before and after time-resolved measurements by recording FT-IR spectra. All measurements were performed at room temperature conditions (22 ± 0.5 °C).

2.4. Computational Details: Force-Field Molecular Dynamics Simulations. Five force-field molecular dynamics (MD) simulations of one 7HQ molecule solvated in 494 methanol (CH_3OH) molecules and cesium formate ($HCOO^-Cs^+$) ion pairs, corresponding to values in Table 1,

Table 1. Parameters Used for the Simulated Systems Including: Concentration of $HCOO^-Cs^+$, number of $HCOO^-Cs^+$ Ion Pairs, Simulation Box Lengths, and Simulation Box Densities

concn [M]	no. of ion pairs	box lengths [Å]	final box densities [g/mL]
0.0	0	33.10	0.73
0.5	10	33.43	0.79
1.0	20	33.77	0.84
2.0	40	34.46	0.94
4.0	80	35.80	1.09

have been performed by the LAMMPS program package.[49] The initial configurations were prepared by PACKMOL.[50] For methanol and the Cs^+ ions, the OPLS-AA (Optimized Potentials for Liquid Simulations all-atom) force-field[51] was used whereas, for 7HQ and the $HCOO^-$ ions, all-bonded interactions and Lennard-Jones parameters were adapted from OPLS-AA. The partial charges were obtained from quantum mechanical calculations using the restrained electrostatic potential (RESP) methodology.[52] All charges in the system were scaled down by a factor of 0.8 to account for screening effects.[53] The simulation step was set to 0.5 fs in all cases. Neither bonds nor angles were constrained. Lennard-Jones interactions and short-range Coulomb interactions were computed up to a cutoff distance of 0.8 nm. Long-range Coulomb interactions were computed by using the particle−particle-particle-mesh approach as implemented in LAMMPS.

In order to equilibrate the system most efficiently regarding particle density and molar distribution, we have applied an equilibration protocol with multiple consecutive steps, prior to starting the production run. The velocities were initialized to 500 K according to the Maxwell−Boltzmann distribution. After an initial equilibration run in the NVT ensemble for 25 ps with temperature rescaling, the temperature was reduced to 300 K during a 100 ps run, in which the temperature was controlled by a Nosé−Hoover chain thermostat[54−56] using a coupling constant of 100 fs. The next step was to change the ensemble from *NVT* to *NpT*. The pressure was controlled by a Nosé−Hoover barostat with a coupling constant of 2 ps. After an *NpT* run of 100 ps, a Langevin dynamics run of 2 ns followed to damp acoustic shock waves that resulted from the system size change. Subsequently, an *NpT* run of 5 ns was computed and the system density was averaged over the simulation. In another step, the ensemble was switched back to *NVT* and the simulation cell was resized to match the average density from the *NpT* run before. After another Langevin dynamics run for 1 ns, a last equilibration of 1 ns followed. In the last step, a production run of 85 ns was performed.

All trajectory analyses were performed by the TRAVIS program package.[57,58] The radial distribution functions (RDFs) plots in figures were created with Xmgrace while the combined distribution functions plots (CDFs) were created by Gnuplot. The molecules and spatial distribution functions (SDFs) were provided by VMD[59] and Tachyon.[60]

https://dx.doi.org/10.1021/acs.jpca.0c10191
J. Phys. Chem. A 2021, 125, 1845−1859

3. RESULTS

3.1. Steady-State Spectroscopy Results. We first investigate the acid−base equilibria with 7HQ and $HCOO^-Cs^+$ in methanol solutions by means of electronic absorption and fluorescence emission measurements. It was shown that in aqueous solution, a significant fraction of the neutral 7HQ conformer N converts into its zwitterion tautomer Z in the ground state.[42,48] In protic alcohol solvents like methanol, this conversion is less likely to happen due to a lower solvent polarity and changes in hydrogen bonding interactions between the chromophore and the solvent. We selected $HCOO^-Cs^+$ as the proton acceptor because of its moderate basicity and high solubility of 8.5 mol/L (M) in methanol at ambient temperature. Figure 2 shows the UV−vis

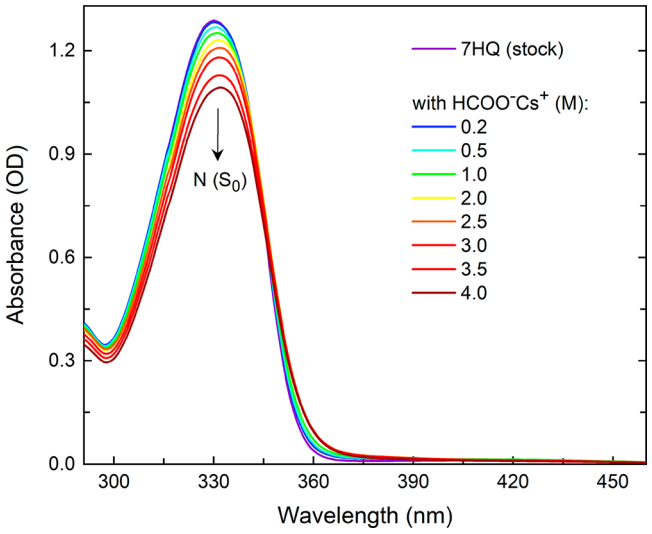

Figure 2. UV−vis electronic absorption spectra of a 50 mM 7HQ solution in CD_3OD as a function of the $HCOO^-Cs^+$ concentration. 7HQ remains predominantly in its N tautomer form. The absorbance decrease upon increasing $HCOO^-Cs^+$ concentration is caused by a density effect at molar base concentrations.

spectra of 7HQ in CD_3OD (defined as stock solution) compared to 7HQ solutions with a progressive increase of the $HCOO^-Cs^+$ concentration as well as the normalized fluorescence emission of the N*, A*, and Z* species of 7HQ. For the stock solution, the absorption peak maximum is located at 330 nm and gets slightly red-shifted by 2 nm for a 4 M concentration of $HCOO^-Cs^+$. The absorption band at 330 nm has been assigned to the N → N* excitation of 7HQ and has a $\pi \rightarrow \pi^*$ character.[61] An additional change we observe in our UV absorption spectra is the reduction of the optical density by approximately 15% for the 7HQ solution with 4 M $HCOO^-Cs^+$ compared to the stock solution. This decrease in absorption is merely a volume change effect, by adding $HCOO^-Cs^+$ at high molar concentration to a methanol solution. For this high concentration of salts or acids, one would anticipate to observe the absorption bands of the A* (maximum at 367 nm) or C* (maximum at 355 nm) charged forms of 7HQ, as observed and calculated by Hoffmann et al. in methanol solutions when strong bases or acids such as NaOH or H_2SO_4[47] had been added. Moreover, we have not observed the appearance of the absorption band of the Z* tautomer, which is expected to appear around 400 nm, as reported by Bardez[42] in an aqueous environment and also by Ekimova et al. in water−methanol solvent mixtures.[48] As a quantitative formation of the 7HQ A, C, or Z species is not apparent even for $HCOO^-Cs^+$ concentrations as high as 4 M, we conclude that the N species dominates for 7HQ in the S_0 state. This allows us to fully explore the photophysics of 7HQ as a function of base concentration when performing time-resolved UV/IR pump−probe measurements.

The excitation of 7HQ in solution at 330 nm leads to a dual fluorescence emission of the N* and Z* species with emission band maxima at 382 and 520 nm, respectively (see Figure 3a,b), in accordance to previous observations of Park et al. in methanol solution.[62] These observations clearly show that an equilibration occurs between the 7HQ N* and Z* species, characterized by an efficient excited-state proton transfer between these two tautomers of 7HQ in the S_1 state in protic solvent media. Now, by adding up to 4 M $HCOO^-Cs^+$ to the 7HQ solution, two major changes occur: a decrease of N* emission to zero, a persistence of Z* emission without a significant intensity change, and a major increase of an emission band strongly overlapping with but clearly located at lower wavelengths from the Z* emission band. Lee and Jang observed a peak at 480 nm in aqueous solutions with 7HQ, and they attributed it to the fluorescence emission of A* species.[63] Hoffmann et al. have attributed an emission band located at 470 nm by direct excitation of the 7HQ anionic A species to its A* fluorescence transition, even though the overall emission is dominated by the Z* tautomer.[47] We notice that fluorescence emission of Z* species prevails for low concentrations of $HCOO^-Cs^+$ while the fluorescence emission of A* species becomes the dominant contribution when increasing the $HCOO^-Cs^+$ concentration to 4 M. Our results clearly show a shift in equilibrium between the N*, A*, and Z* species of 7HQ in the electronic excited state, with the A* contribution becoming the dominant one at high base concentrations. To further disentangle the spectrally overlapping but distinct A* and Z* emission bands, we have applied second derivative calculations on the measured fluorescence emission spectra.[64] We used the "differentiate function" in Origin to convert the raw fluorescence spectra into their second derivatives. As for the first step, we transformed the raw spectra into their first derivatives to find possible detectable peaks and the corresponding residuals coming out from this calculation. The values with their reciprocal residuals that increased above the threshold of the second-order residuals were considered as hidden peaks. Then, we calculated the second derivative of the raw fluorescence spectra to enhance even further the small contributions of these hidden peaks, thus increasing the possibility to detect the contributions coming from different molecular species (of 7HQ, in this case). The decomposed spectral contributions $d^2F/d\lambda^2$ are shown in Figure 3c and involve the second-order derivative of raw fluorescence (F) as a function of detection wavelength λ. The two resulting negative peaks can be assigned to the fluorescence bands of N*, A*, and Z*, with emission maxima located at 370, 462, and 520 nm, respectively. Further, we notice that the second derivative spectra indicate that the spectral shape and location of the fluorescence bands of the neutral N* and Z* tautomers are not significantly affected upon an increase of the $HCOO^-Cs^+$ concentration. In contrast, the second derivative spectra show a spectral shift of the A* species emission band. This may be an indication of a larger interaction between the 7HQ-A* anion with the charged ions of $HCOO^-Cs^+$, which we tentatively ascribe to

https://dx.doi.org/10.1021/acs.jpca.0c10191
J. Phys. Chem. A 2021, 125, 1845−1859

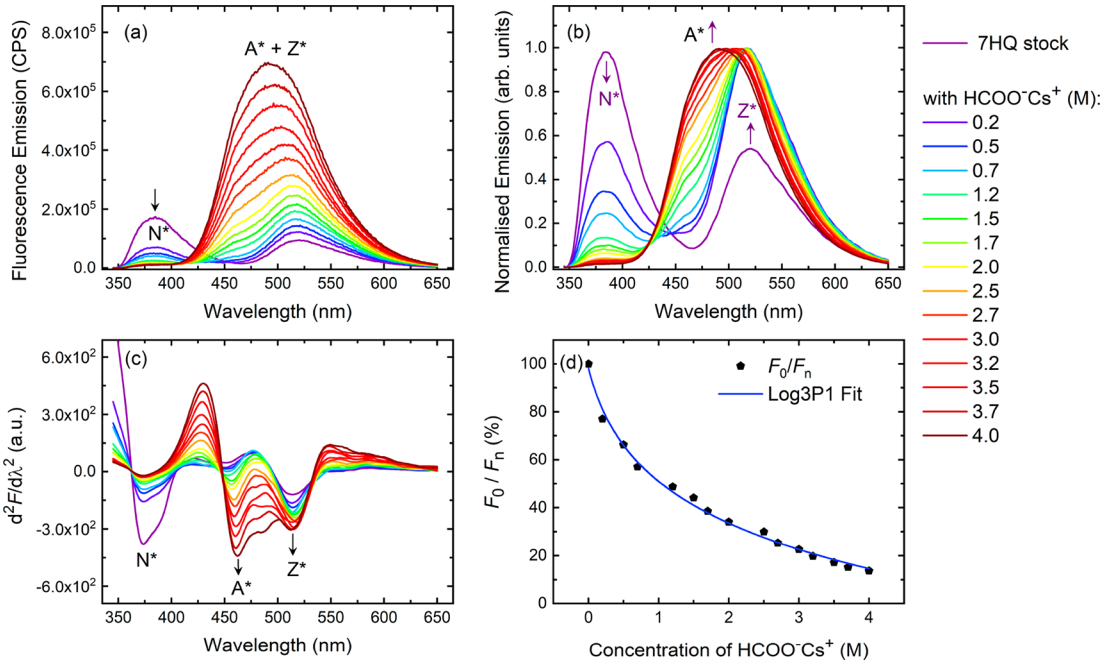

Figure 3. (a) Measured fluorescence emission spectra (excitation with 330 nm) for 1 mM 7HQ solution in CD_3OD solvent with an increasing concentration of $HCOO^-Cs^+$ as indicated in the plot. (b) Fluorescence spectra normalized to their maximum intensity value. (c) Corresponding second derivative spectra showing the relevant peaks. (d) Ratio between the fluorescence of 7HQ stock solution, without $HCOO^-Cs^+$ (F_0) to the fluorescence emission of 7HQ in the presence of $HCOO^-Cs^+$ (F_n) as a function of base concentration n. Log3P1 is a logarithmic transform calibration function of the form $y = a - b \times \ln(x + c)$, with derived values for the coefficients $a = 57.8 \pm 2.26$, $b = 29.8 \pm 1.72$, and, $c = 0.26 \pm 0.05$.

Coulomb interactions between the positive and negative charges between the ions. We also plotted in Figure 3d the ratio of the fluorescence emission of 7HQ in methanol without $HCOO^-Cs^+$ F_0 to that of 7HQ solutions F_n with increasing $HCOO^-Cs^+$ concentration n and observed a logarithmic behavior. We used the logarithmic transform calibration function Log3P1 from Origin to convert the skweded data into a normal distribution.

3.2. Femtosecond UV/IR Pump−Probe Results on 7HQ and Formate Solutions. We have explored the proton transfer dynamics of 7HQ in deuterated methanol (CD_3OD) with different amounts of $HCOO^-Cs^+$ by monitoring the IR-active vibrational marker modes of the different charged species of 7HQ in the first electronic excited state and of formic acid by use of ultrafast UV/IR pump−probe spectroscopy. For this, we have investigated the spectral regions between 1400−1550 cm^{-1}, with which we are able to measure the kinetics of the N*, Z*, and A* through the respective fingerprint modes,[47,48] and between 1640 and 1760 cm^{-1}, where the formation kinetics of HCOOD can be determined by its C═O stretching mode. Figure 4 shows the comparative overview of the transient UV/IR spectra obtained for different $HCOO^-Cs^+$ concentrations at designated pulse delay times for the two spectral regions. Here we assign the transient IR marker bands as reported previously.[47,48]

Figure 4 shows the kinetics of 7HQ in CD_3OD, where the deuteron transfer dynamics of N* is indicated by the decay of its marker band at 1473 cm^{-1} with a time constant of 360 ps. This is correlated with the rise of the Z* tautomer, as shown by the 1437 and 1529 cm^{-1} bands, whereas the C* cationic form is not apparent in the transient UV/IR spectra, due to a lack of a significant transient population buildup of C* in the N* → C* → Z* pathway.[47,48] Increasing the $HCOO^-Cs^+$ concentration leads to the following observations: (a) The initial

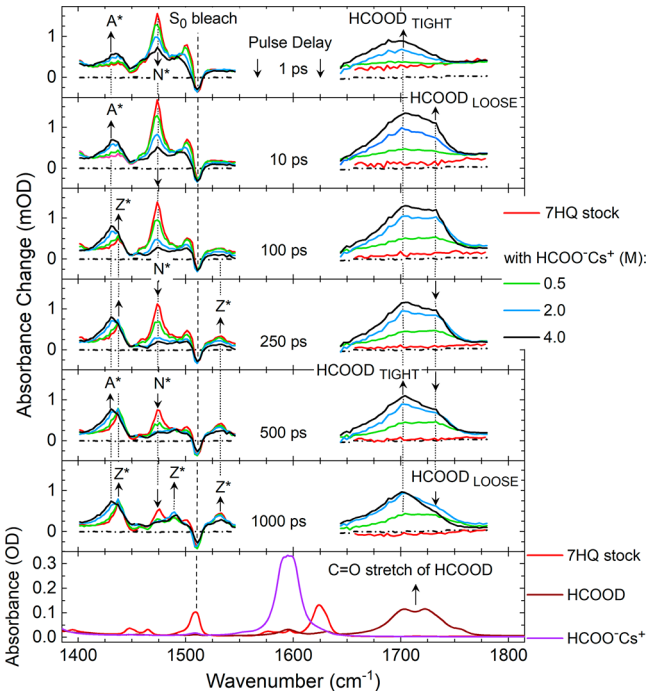

Figure 4. Comparison of the transient UV/IR pump−probe spectra monitoring the fingerprint modes of the N*, A*, and Z* species of photoexcited 7HQ, and of formic acid HCOOD, in CD_3OD solution as a function of $HCOO^-Cs^+$ concentration, at particular pulse delay times. The stock solution had been prepared with 50 mM 7HQ in CD_3OD. The lowest panel shows the steady-state FT-IR spectra of 7HQ, HCOOD, and $HCOO^-Cs^+$ in CD_3OD.

signal strength of the 1473 cm^{-1} band of N* decreases with increasing base concentration, within time resolution of the

https://dx.doi.org/10.1021/acs.jpca.0c10191
J. Phys. Chem. A 2021, 125, 1845−1859

experiment (~0.4 ps). (b) A new band located at 1435 cm^{-1}, also appearing within time resolution, gets more intense with increasing base concentration. (c) Subsequent changes in the transient UV/IR spectra at longer pulse delay show a more complete diminishing of the N* marker band at 1473 cm^{-1} and a less strong appearance of marker bands at 1438 and 1529 cm^{-1} indicative of Z* (but a small band at 1490 cm^{-1} that can also be assigned to Z* is more apparent at long pulse delay times, for the higher base concentration cases). (d) Instead, for the higher base concentrations of 2−4 M, the marker band initially appearing at 1435 cm^{-1} appears to show on a time scale of several picoseconds a frequency downshift to 1430 cm^{-1}. This marker band can be assigned to the A* anionic charged form of 7HQ. (e) An appearance of a 53 cm^{-1} (fwhm) broad band centered at 1700 cm^{-1}, located in the C═O stretching spectral region, indicative of the formation of formic acid HCOOD within time resolution, is observed at high base concentration. (f) At larger pulse delay, an additional frequency upshifted band at 1736 cm^{-1} appears on picosecond time scales but decreases strongly at subnanosecond pulse delay times for the highest base concentrations used (see also Figure 5), whereas a band located around 1700 cm^{-1} remains

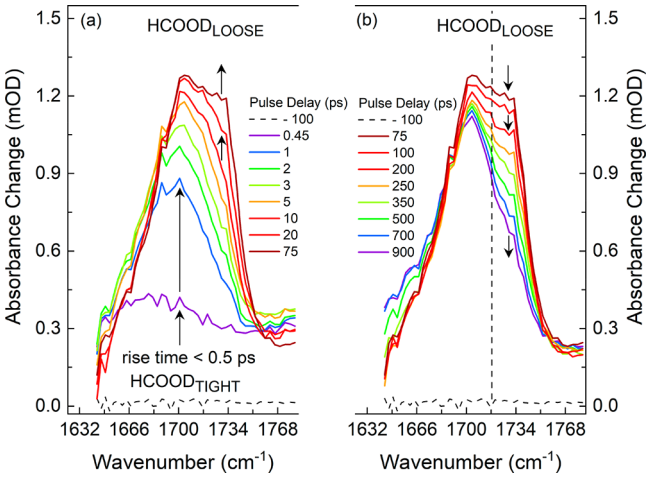

Figure 5. Blow-up of the C═O stretching region, showing components emerging within time resolution, early time contributions appearing on a time scale of 15−50 ps, and long time scale disappearance of the high-frequency component on a time scale of 500−600 ps.

persistent as long as 1 ns (the maximum scanning range of our pulse delay stage). As already hinted at with the markedly different fluorescence emission characteristics of 7HQ upon increased $HCOO^-Cs^+$ concentration, we conclude that the observations from our femtosecond UV/IR pump−probe measurements confirm that the proton transfer dynamics of 7HQ in CD_3OD can be steered away from the N* → C* → Z* pathway[47,48] when molar concentrations of $HCOO^-Cs^+$ are present in solution. The observation of both A* and HCOOD species generated at (sub)picosecond pulse delay times suggest a quantitative change where 7HQ follows the N* → A* reaction path. The question now is whether further reaction dynamics occur after this first step, for instance, whether the conversion of A* → Z* is a significant event under the sample conditions investigated here.

Further insight into possible distinct reaction pathways taken by 7HQ when $HCOO^-Cs^+$ is added to the CD_3OD solution is provided when we inspect the time dependence of the femtosecond UV/IR pump−probe signals at the marker mode frequencies. Figure 6a shows the temporal behavior of the marker modes indicative of the 7HQ N* and Z* tautomers, at 1473 and 1437 cm^{-1}, respectively. Whereas the decay of N* appears to increase its rate with a single exponential decay time constant of 370 ps without base to 5−50 ps (using biexponential fits) for the highest formate concentration measured Figures 6b−e, the rise of Z* continues to show a long rise time even increasing from ~370 ± 30 to 540 ± 60 ps, albeit the relative magnitude of Z* contributing to transient absorbance changes diminishes with respect to that of the A* anion species, which has its marker band at 1430 cm^{-1} at large pulse delay times. While a marker band of Z* at 1490 cm^{-1} only becomes clearly observable at large pulse delay times of hundreds of picoseconds (at early pulse delay times spectral overlap with the large N* marker mode dictates the transient UV/IR pump−probe signals), its slow rise with a time constant of ~550−650 ps is in close resemblance to the decay of the high-frequency component of the C═O stretching band of HCOOD, which in itself appears on a time scale of ~10−15 ps for the highest base concentration (Figures 6f−j).

These results hint at the complexity of the three-species reaction dynamics, where 7HQ, formate/formic acid, and methanol, in principle are all involved in acid−base chemistry, with 7HQ having two sites, the proton-donating hydroxyl group and the proton-accepting quinoline N site. The relative importance of the possible reaction pathways and microscopic proton transfer steps can change upon the variation of the relative concentrations of the reactive species. To obtain further insight into this, we now investigate possible preferences of relative positions of the formate anions, cesium cations, and methanol solvent molecules around 7HQ.

3.3. Molecular Arrangements around 7HQ. The force-field molecular dynamics simulations have provided us additional information about the spatial distribution function of methanol (MeOH) and cesium formate ($HCOO^-Cs^+$) in the vicinity of 7HQ. First, the spatial distribution functions (SDFs) have been calculated and are shown in Figure 7. The SDFs indicate the probability of finding different particles at a certain position in space around a fixed reference system. Looking at Figure 7a,b, we can observe where the formate and cesium ions are found with the highest probabilities. The formate anion, $HCOO^-$ (blue isosurface), mainly appears near the hydrogen of the hydroxyl group of 7HQ (7HQ-OH) in a double layer that represents the two oxygen atoms of formate. Observing this double layer twice, we conclude that the 7HQ-OH hydrogen is preferentially oriented in the plane of the aromatic ring system of 7HQ. The space between those layers shows a high probability of finding the cesium cation (Cs^+), represented by the red isosurface. There is a high probability of finding the Cs^+ near the nitrogen atom of 7HQ (N-site) that is partially negatively charged and can interact with Cs^+. Figure 7c,d shows that the hydroxyl group of MeOH is found near the 7HQ-OH group with the highest probability as well. Due to the two preferred positions of 7HQ-OH, either as *trans*-7HQ (Figure 7a,c) or *cis*-7HQ (Fogure 7b,d), the Me−OH molecule can also interact in two distinct ways with 7HQ-OH. Observing that there is a high probability for both $HCOO^-$ and −OH of MeOH to interact with 7HQ-OH, we can conclude that both oxygens of $HCOO^-$ and of MeOH are

https://dx.doi.org/10.1021/acs.jpca.0c10191
J. Phys. Chem. A 2021, 125, 1845−1859

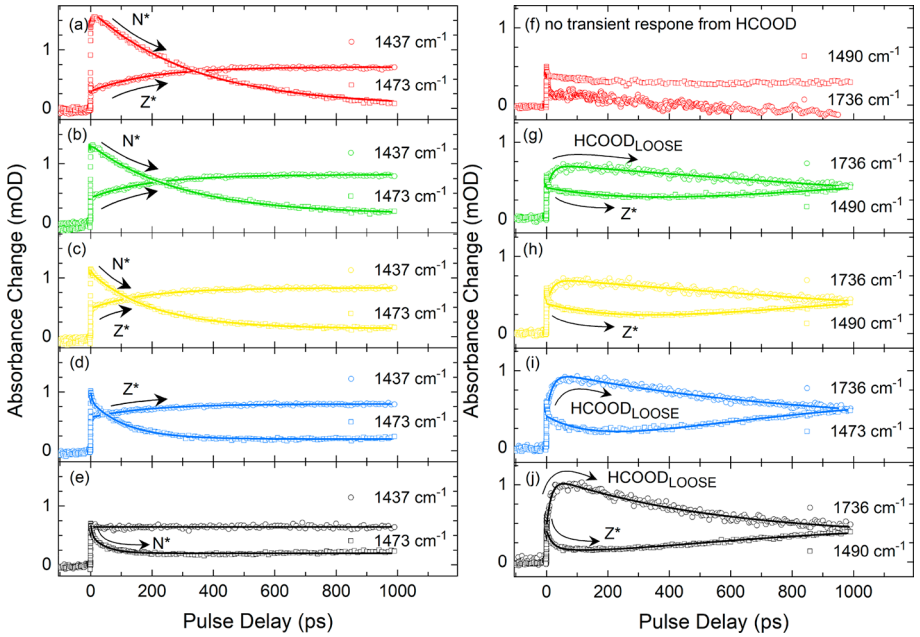

Figure 6. Temporal characteristics of the transient absorbance at designated detection frequencies marking the kinetic behavior of N*, Z* and HCOOD species, as described in the text, as a function of $HCOO^-Cs^+$ concentration: 7HQ in CD_3OD (black curves), 0.5 M base (red curves), 1.0 M base (orange curves), 2.0 M base (green curves), 4.0 M base (purple curves). Solid curves are multiexponential fits to the experimental data (dots).

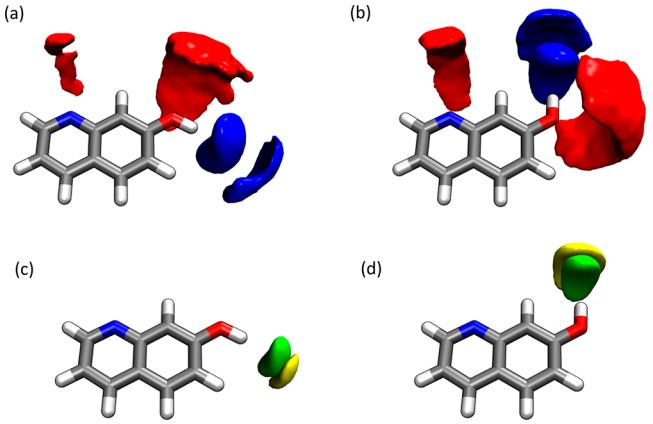

Figure 7. Spatial distribution functions (SDFs) of *trans*-7HQ (a,c) or *cis*-7HQ (b,d) with 2.0 M of $HCOO^-Cs^+$ (a,b) and MeOH (c,d) around 7HQ where the red is the isosurface: Cs^+ cation; blue, O_{HCOO^-}; yellow, H_{OH} of MeOH; green, O_{OH} of MeOH. Isovalues: 1.5 nm^{-3} for Cs; 3.0 nm^{-3} for formate; 25 nm^{-3} for O and H of MeOH.

readily available as acceptor sites for the acidic proton of the photoexcited 7HQ.

For a more quantitative analysis of the preferred binding directions of the three components of the solvent around the solute, we have projected the distribution functions on the molecular plane of 7HQ. Figure 8 shows the average particle density of MeOH (Figure 8a,b), of the $HCOO^-$ anion (Figure 8c,d), and of the Cs^+ cation (Figure 8e,f) at a given position relative to the uniform density where the average particle density is depicted by the color scale of the plots. Here, we examine a plane projection of the simulation cell defined by the 7HQ ring plane. Values below 1 indicate a depletion of the molecule while values larger than 1 indicate that the molecule is more often found at a specific rather than at an arbitrary position. In Figure 8a,b it can be seen that the highest particle density of MeOH is close to that of 7HQ-OH and that MeOH interacts with 7HQ at this position with its oxygen atom since on average the −OH group of MeOH points away from 7HQ. However, between those two maxima, the −OH group of MeOH is orientated in the opposite direction. Considering the environment of the N atom of 7HQ, another weak interaction with MeOH can be observed where the −OH of MeOH points on average to the 7HQ molecule. Figure 8c,d shows the orientation of the $HCOO^-$ anion around 7HQ. The highest average particle density is found next to the 7HQ-OH group as well. The $HCOO^-$ anion points with its oxygen atoms to the 7HQ molecule. However, we find another maximum of the average particle density between the lipophilic hydrogen atoms of the opposite side of 7HQ and the $HCOO^-$ anion. This indicates a weak solvation layer of $HCOO^-$ anions around the lipophilic parts of 7HQ where the $HCOO^-$ points with its hydrogen atoms toward the 7HQ molecule. Then, the average particle density of Cs^+ cations around 7HQ is illustrated in Figure 8e,f. Maxima were found near the −OH group and the quinoline N atom of 7HQ. Although there are fewer Cs^+ cations found near the 7HQ-OH compared to MeOH and the $HCOO^-$ anion, the average particle density next to the quinoline N atom is the highest among those three molecules. Whereas Cs^+ does not have an orientational preference, the formate anion has a preferred orientation akin to its hydrogen bonding interactions with the 7HQ-OH group. As such, a formate anion is located in the solvent for *trans*-7HQ (where the 7HQ hydroxyl O−H bond vector points away from the 7HQ aromatic ring system) or is part of a proton relay pathway (together with methanol solvent molecules) that bridges the quinoline N site with the OH group of *cis*-7HQ (where the O−H bond vector points in the direction of the proton relay bridge).

Knowing that both MeOH solvent and the $HCOO^-$ anion favor hydrogen bonding with 7HQ, an interesting indication would be if there is a probability to form specific molecular

https://dx.doi.org/10.1021/acs.jpca.0c10191
J. Phys. Chem. A 2021, 125, 1845−1859

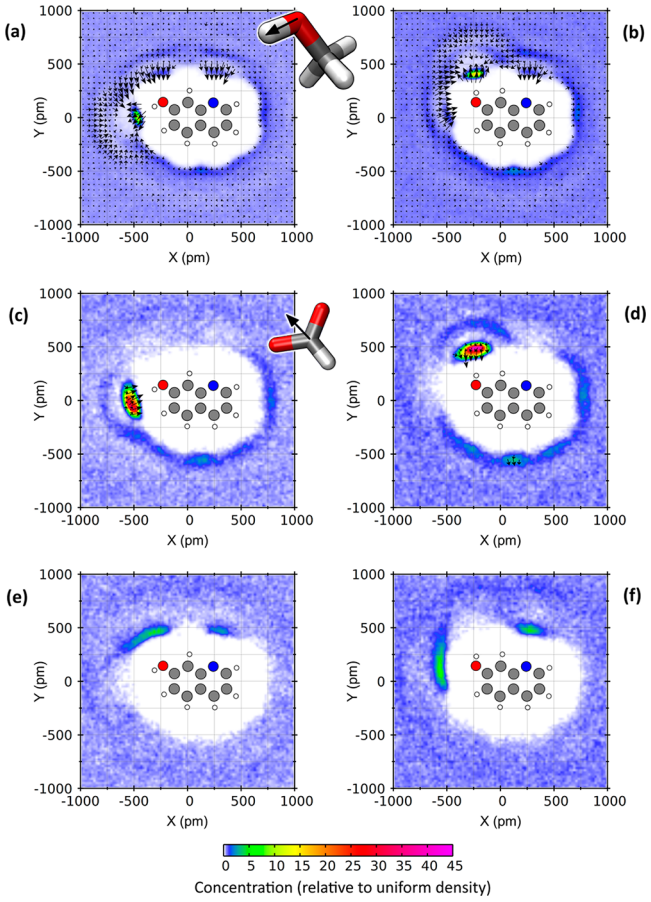

Figure 8. Average particle density of MeOH molecules (a,b), $HCOO^-$ anion (c,d), and Cs^+ cation (e,f) around a *trans*-7HQ molecule (a,c,e) or *cis*-7HQ molecule (b,d,f) (see the color scale) together with the average orientation of (a) the O−H bond vector of MeOH and (b) center of mass vector of the $HCOO^-$ anion (both indicated as arrows) in a simulation of 7HQ and 2.0 M of $HCOO^-Cs^+$ dissolved in MeOH.

geometries where the $HCOO^-$ and the 7HQ-OH group are separated by a MeOH molecule (i.e., "solvent-separated" or "loose-reactive" complexes) or when the 7HQ-OH is directly hydrogen bonded (i.e., "contact pairs" or "tight-reactive" complexes) to one of the oxygen atoms of the $HCOO^-$ anion. To investigate whether this is possible, we show in Figure 9 the combined distribution function (CDF) of the radial distribution function (RDF) between the hydrogen atom of 7HQ-OH and the oxygen atom of MeOH and of the RDF between the hydrogen of MeOH and the oxygen atoms of $HCOO^-$ anion. We observe the highest maximum at a distance of approximately 180 pm on both axes. The CDF peak at 180 pm for both $H_{MeOH}\cdots O_{7HQ}$ and $H_{MeOH}\cdots O_{Formate}$ means actually a "loose" complex with MeOH closer than formate to the 7HQ-OH group. Instead, the extended peak at 290−500 pm (and beyond) for $H_{MeOH}\cdots O_{7HQ}$ and confined to values around 180 pm for $H_{MeOH}\cdots O_{Formate}$ has contributions from "tight" complexes. The peak confined to values around $H_{MeOH}\cdots O_{7HQ}$ and extended from 350−420 pm around and $H_{MeOH}\cdots O_{Formate}$ is indicative of configurations for "loose" configurations as well. This analysis of the CDF indicates that both "loose-reactive" and "tight-reactive" molecular arrangements are possible and correlate well with our experimental results.

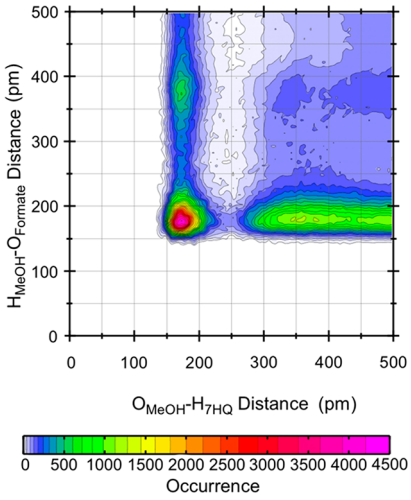

Figure 9. Combined distribution function depicting the distance between the hydrogen atom of 7HQ-OH and the oxygen atom of MeOH as well as the distance between the hydrogen atom of the −OH group of MeOH and the oxygen atoms of $HCOO^-$ in a system with a concentration of 2.0 M of $HCOO^-Cs^+$.

4. DISCUSSION

4.1. Early and Late Time Dynamics of 7HQ−Formate Acid−Base Reaction Pairs. From our classical MD simulations as presented in the previous section we conclude that for high $HCOO^-Cs^+$ concentrations the formate anion has a high likelihood to be in close proximity of the proton-donating −OH group of 7HQ. These configurations can be regarded as "contact" (or "tight") acid−base reaction pairs. A significant fraction of configurations have been identified where a methanol molecule has been found between the proton-donating −OH group of 7HQ and the formate anion base, which are reminiscent of the "solvent-separated" (or "loose") acid−base reaction pairs. These molecular arrangements occur irrespective of the orientation of the −OH group with either the formate anion pointing in the direction of the 7HQ quinoline N site, or away from 7HQ into the bulk solution. "Tight" and "loose" acid−base reaction pairs have been postulated to explain the ultrafast contributions in photoacid−base neutralization dynamics in aqueous solution.[37−40] This raises the question whether such "tight" and "loose" acid−base reaction pairs can also be observed in our time-resolved measurements of the reaction dynamics of 7HQ−formate in dissolved methanol. In addition to that, when comparing water and methanol as solvent, the roles should be considered of the difference in solvent polarity, and of the concentrations of $HCOO^-Cs^+$ used in the experiments, being relatively high compared to that of the solvent.

Figure 10 shows the transient IR spectra of 7HQ recorded at 1 ps, 10 ps, and 1 ns, of our 7HQ stock solution, and for solutions with $HCOO^-Cs^+$ base added to the solutions, by using identical excitation and detection conditions. The magnitude of the 1473 cm^{-1} marker mode at a particular pulse delay time is a direct indication of the transient population of 7HQ-N*. We observe a significant decrease of the signal strength of this marker mode within time resolution. This initial decrease is a direct measure for those 7HQ-N−formate complexes that promptly react upon electronic excitation, in a barrierless deuteron transfer reaction, much akin to the "tight" photoacid−carboxylate complexes in

https://dx.doi.org/10.1021/acs.jpca.0c10191
J. Phys. Chem. A 2021, 125, 1845−1859

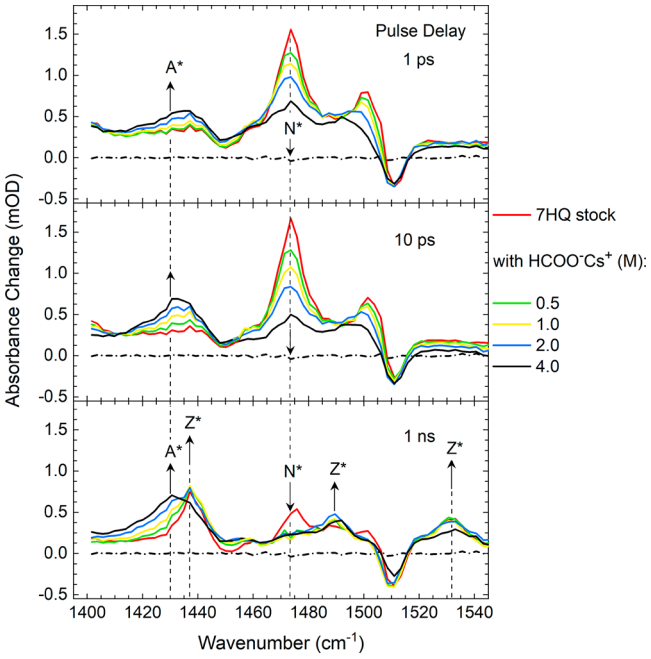

Figure 10. Comparison of transient UV/IR pump−probe spectra of 7HQ in CD_3OD measured at 1 ps, 10 ps, and 1 ns pulse delay times for different $HCOO^-Cs^+$ base concentrations. Dotted lines are reference lines denoting the frequency positions of N* (1473 cm^{-1}), Z* (1437 cm^{-1}), and A* (1430 cm^{-1}) 7HQ species.

aqueous solution reported before.[37−40] These "tight" 7HQ-N−formate complexes are also evident when one inspects the frequency positions of the 7HQ-A* and formic acid marker modes observed at these early pulse delay times. For 7HQ-A* the marker band is initially centered around 1435 cm^{-1} whereas the early time component of HCOOD is located at 1697 cm^{-1}. This shows that the "tight" 7HQ-N*−formate acid−base reaction pair converts by an ultrafast deuteron transfer within 0.5 ps, after which it remains in a "tight" 7HQ-A*−HCOOD conjugate base−conjugate acid product pair at picosecond times. Table 2 summarizes to what extent this fraction of "tight" 7HQ-N−formate complexes becomes significant at molar concentrations of base in CD_3OD solution.

Table 2. Fraction of N_{free}, N_{tight} and N_{loose} as Derived from the 1473 cm^{-1} N* Marker Mode Kinetics

concn of $HCOO^-Cs^+$ (M)	$N_{free/remote}$ (error margin ±0.05)	N_{tight} (error margin ±0.04)	N_{loose} (error margin ±0.02)
0	1		
0.5	0.73	0.22	0.05
1.0	0.59	0.32	0.09
2.0	0.42	0.44	0.14
4.0	0.18	0.66	0.16

Having concluded that the femtosecond UV/IR pump−probe spectra and the CMD simulations indicate that a major fraction exists of "tight" 7HQ-N*−formate acid−base reaction pairs, we now explore the possibile occurrence of "loose" 7HQ-N*−formate acid−base reaction pairs, indeed also suggested by the CMD simulations to occur. Besides an early decrease of 7HQ-N* with a time constant faster than the time resolution in the experiment, the subsequent further decay of transient population of 7HQ-N* occurs on a multitude of time constants (with time constants ranging from the few picoseconds to tens to hundreds of picoseconds). From the photoinduced neutralization reactions of 8-hydroxy-pyrene-1,3,5-trisulfonate (HPTS) and carboxylate bases in aqueous solution it has been concluded that such "loose" HPTS−carboxylate acid−base reaction pairs in D_2O have an overall deuteron transfer from the photoacid via the intermediate water solvent molecule to the carboxylate base with time constants on the order of 5−10 ps,[38−40] in accordance to free energy-reactivity correlations (also known as Marcus proton transfer plots) for proton transfer reactions in protic solvents.[27,34,40,48,65] When considering pK_a values as reported[66−68] or deduced for 7HQ-N* and formic acid in deuterated methanol, we find that these free energy-reactivity relationships[27,40,65,69−72] predict deuteron transfer time constants for the 7HQ-N*−formate acid−base reaction pair in CD_3OD on the order of 5 ps. Certainly, limitations in this approach should be anticipated when assuming that the high molar salt solutions investigated in this study obey the infinite dilution conditions for the semiempirical approach of the free energy-reactivity correlations using bulk solution pK_a values. Nevertheless, using this finding, we estimate that the "loose" 7HQ-N*−formate acid−base reaction pairs, reacting within 10 ps, make up a clearly smaller fraction in the (sub) molar $HCOO^-Cs^+$ base solutions (see Table 2). As a result, the remaining 7HQ-N* molecules we assign as "free/remote", with the premise, which in the high molar base solutions these will react eventually with formate (hence "remote"), after "mutual diffusion" between 7HQ-N* and the formate anion, that may well, rather than a clear diffusional motion over extended distances, involve small rearrangements of formate anion, Cs^+ counterions, and the most nearby solvent molecules, to accommodate a proton transfer on a few tens of picosecond time scales.

Another indication for the occurrence of "loose" 7HQ-N*−formate acid−base reaction pairs can be found in the transient response in the C=O stretching region (see Figure 5). After the rise of a band at 1700 cm^{-1} within time resolution, the transient UV/IR pump−probe spectra show that a second band appears at 1736 cm^{-1} with a 15−50 ps time constant. The observation of a two-component structure of C=O stretching modes may have different underlying origins, such as (a) Fermi resonances, often observed for carboxylic acids; (b) different magnitudes of frequency shifted C=O stretching mode components with varying degrees in hydrogen bonding interactions; (c) frequency shifts imposed by electrical field interactions of surrounding polar solvent molecules or ions. For both (b) and (c) a frequency shift due to a change in hydrogen bonding or (local) electrical field interactions may affect the shape of vibrational transitions split by Fermi resonances. Figure 11 shows how the C=O stretching band of formic acid changes upon $^{12}C/^{13}C$ or H/D isotope exchange, and solvent medium. While formic acid forms cyclic dimers in CCl_4 and cyclohexane, in the polar solvents acetonitrile, DMSO, methanol, and water, the FT-IR spectra are dominated by formic acid monomers hydrogen bonded with the solvent molecules. Fermi resonances, the coupling between a v = 0 quantum state of one vibrational mode to a v = 2 quantum state of a second vibrational mode, typically lead to a mixing of these two states, where an overtone v = 0 → v = 2 forbidden transition obtains an increase in transition cross section from a strongly allowed fundamental v = 0 → v = 1 transition, leading to a marked splitting and reshaping of the transition bands.

https://dx.doi.org/10.1021/acs.jpca.0c10191
J. Phys. Chem. A 2021, 125, 1845−1859

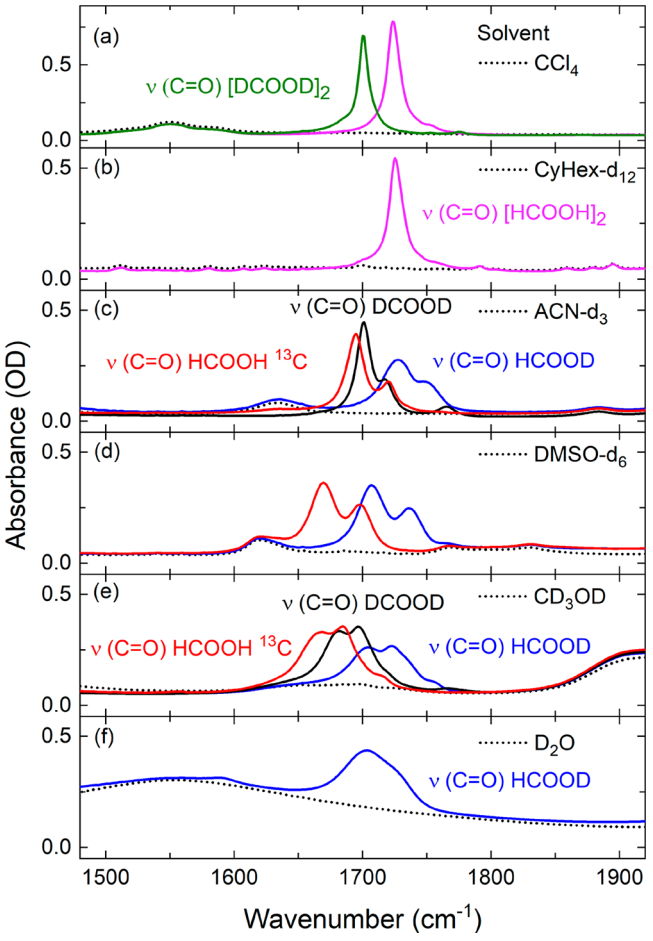

Figure 11. FT-IR spectra of the C═O stretching vibration of different isotopomers of formic acid (HCOOH, DCOOD and $H^{13}COOH$) dissolved in CCl_4 (a), cyclohexane-d_{12} (b), acetonitrile-d_3 (c), DMSO-d_6 (d), CD_3OD (e), and in D_2O (f). The concentration of HCOOH and $H^{13}COOH$, $H^{13}COOD$, and DCOOD is 0.3 M for all measurements.

Small frequency shifts, due to e.g., changes in hydrogen bonding interactions, lead to marked different magnitudes of Fermi resonance interactions and, thus, in the IR-active spectra. However, for formic acid we find that the $^{12}C/^{13}C$ isotope and H/D substitutions only lead to net frequency downshifts, without substantially changing the shape of the C═O stretching peak patterns. From these observations we conclude that Fermi resonances as such are not the main interaction underlying the peak splitting observed for formic acid in polar solvents. Instead, we argue that the distinct difference in peak patterns is due to differences in hydrogen bond interactions in these solvents, with frequency positions governed by solvent polarities and hydrogen bond interaction strengths, and peak intensity differences caused by a different relative ratio in population of the hydrogen bond configurations. This conclusion has been noted before, where the relative orientation of the O—H to the C═O bond vectors, cis vs trans (syn vs anti) are found to differ in C═O stretching frequency on the order of 10−30 cm^{-1}, depending on the solvent medium,[73−76] with the cis (syn) geometry being the predominant species in deuterated acetonitrile and heavy water (80% and 70% in these two solvents, respectively).[75] On the basis of these steady-state FT-IR and ultrafast 2D-IR spectroscopic results, we conclude that for our measurements the observation of a two-component structure of the C═O stretching band with a different temporal behavior is a strong indication for two different configurations of HCOOD. The appearance with a 15−50 ps time constant suggests the 1736 cm^{-1} band is due to HCOOD formed in "loose" 7HQ-N*−formate acid−base reaction pairs, with a marked frequency upshift clearly distinct from the HCOOD formed in "tight" 7HQ-N*−formate acid−base reaction pairs within time resolution. Whether this frequency shift is caused by differences in hydrogen bond interactions, in (local) electrical field interactions of the 7HQ chromophore in the A* state, by a differences in relative position in Cs^+ and other formate ions, or by a mere preference of cis (syn) conformations of HCOOD would be an intriguing topic for further research. In addition to that, the subsequent partial decay of this high-frequency C═O stretching component with a 0.5−0.6 ns time constant similar to that of the 7HQ-A* species suggests that a correlation may exist between the underlying mechanisms of the decay of 7HQ-A* and of (a fraction of) 7HQ-A*−HCOOD conjugate base−conjugate acid product pairs.

We are now in the position to distinguish different configurations of 7HQ and formate reaction pairs. In a similar fashion as for HCOOD, 7HQ is known to have two dominant relative orientations of the O−H bond and C−O bond vectors.[77,78] *trans*-7HQ has its O−H group pointing away from the quinoline aromatic ring system into the solvent. For *cis*-7HQ the O−H group is directed toward the quinoline N site. It has been understood that together with protic solvent molecules 7HQ forms a proton relay pathway through which the proton transfer process converts 7HQ-N* into its 7HQ-Z* tautomer.[43,44] Regardless of the nature of the proton transport, either via an excess proton transfer mechanism (7HQ-N* → 7HQ-A* → 7HQ-Z*) or via a proton vacancy transfer mechanism (7HQ-N* → 7HQ-C* → 7HQ-Z*), this proton relay pathway does not constitute a rigid hydrogen bonded network, but rather a solvent bridge with continuously breaking and re-forming hydrogen bonds. The exchange dynamics between *trans*-7HQ and *cis*-7HQ occurs on a much faster time scale than the slowest proton transfer step of 7HQ. Hence the effective proton transfer pathway is that of when 7HQ is in its cis configuration, as this will be the one where the 7HQ-N* → 7HQ-Z* tautomer conversion will be most efficiently fully completed.

Now when formate is added as an additional base, then for both "tight" and "loose" complexes with 7HQ formate the first proton transfer reaction will be much faster than any adjustment of 7HQ to the most efficient proton transfer reaction pathway. Indeed, when formate forms a "tight" complex with *trans*-7HQ-N, the resulting first proton transfer step converts 7HQ-N* + $HCOO^-$ → 7HQ-A* + HCOOD, with formic acid located away from the proton relay pathway. On the time scale of our experiment (maximum pulse delay scanning range 1 ns), it will take too much time for either formic acid to diffuse to the quinoline N site, or upon dissociation for the protons to follow a von Grotthuss-type hopping pathway to the other side of 7HQ-A*. It is a likely next step that 7HQ-A* will in itself convert into 7HQ-Z* by proton abstraction from the methanol solvent molecule nearest to the quinoline N site. Instead, for a "tight" complex between formate and *cis*-7HQ-N, the first step will have the formic acid as part of a possible proton relay pathway. Similar arguments will hold for the "loose" complexes, when one solvent molecule separates the −OH group from the formate anion. It will then

https://dx.doi.org/10.1021/acs.jpca.0c10191
J. Phys. Chem. A 2021, 125, 1845−1859

be not only a question of different contributions to the observed signals, kinetics indicative of transient populations of the different charged forms of 7HQ, i.e., 7HQ-N*, 7HQ-A*, and 7HQ-Z*, and those of HCOOD, but also to what extent these are directly correlated. In particular, a decay of 7HQ-N* and a rise of 7HQ-A* and a rise of HCOOD will show a strong correlation is the proton exchange occurs in the "tight" complexes. This may also be the case for the "loose" complexes provided that the sequential proton transfer steps 7HQ-N* + CD_3OD + $HCOO^-$ → 7HQ-A* + $CD_3OD_2^+$ + $HCOO^-$ → 7HQ-A* + CD_3OD + HCOOD will not be too different with their time scales. Instead, 7HQ reacting with the solvent without any direct involvement of the formate base will be either through the "solvent only" reaction pathway 7HQ-N* → 7HQ-C* → 7HQ-Z* that has been shown to be the dominant pathway in methanol and water/methanol mixtures or, in the case of 7HQ-A*, through the above-mentioned methoxide generation at the quinoline N site, 7HQ-A* + CD_3OD → 7HQ-Z* + CD_3O^-. In either case, the kinetics of signals due to 7HQ-A* and 7HQ-Z* and those of HCOOD will have a negligible degree of correlation in the temporal behavior.

4.2. PCA-SVD Analysis of the UV/IR Pump−Probe Spectra of the Photo-Induced 7HQ−Formate Acid−Base Reaction. Even though proton transfer dynamics among the different charged forms of photoexcited 7HQ, formate anion, and the solvent methanol may appear to be inherently of a complex nature, as is the interplay between formate anion motions to the reactive sites of 7HQ, the hydrogen bond dynamics of the interspersed methanol molecules, and the different routes proton transfer steps can take, we have seen in the previous section that particular photoacid−base reaction pairs, denoted as "tight" and "loose", are apparent in the kinetic behavior of the respective vibrational marker modes. The strong similarities of particular temporal components of these particular vibrational marker modes point at correlated population kinetics. We have further analyzed this aspect by principal component analysis−singular value decomposition (PCA-SVD) of our transient UV/IR pump−probe results. This procedure consists of three steps.[48] First the data matrix (transient spectra) is decomposed into components by the standard SVD routine. The resulting set of singular values is analyzed and the number of significant components is determined. Only components with a few singular values clearly larger than the rest of the spectrum are retained. Based on the number of significant components, a kinetic model is formulated. A least-squares fitting procedure is used to determine linear combinations of the SVD components and the resulting decay or rise rates, corresponding to the kinetic model.

Here we compare the results of 7HQ in CD_3OD (stock solution, no base added) with that of 7HQ with the largest base concentration (4.0 M) in CD_3OD for pulse delay times from 1 ps to 1 ns (the latter the maximum of our delay stage). It turns out that our time-resolved spectral data obtained on both the stock solution and the 4.0 M formate solution have only a few significant kinetic components. As reported before, the stock solution has two components, one representing a broadband featureless contribution due to multiphoton excitation of the solvent and/or cell windows, and another indicative of the decay of N* and rise of Z* (occurring by the hydroxide/methoxide transfer pathway N* → C* → Z*[48]). For the 4.0 M solution we find a three component description satisfactory (see Figure 12).

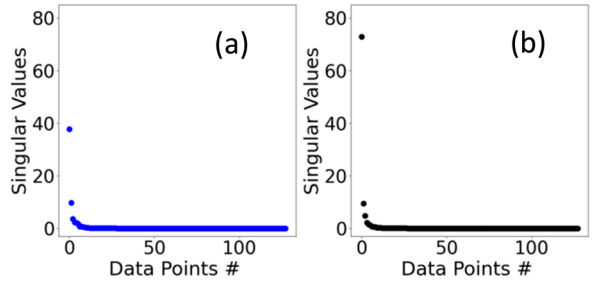

Figure 12. Singular values plots showing the most relevant components extracted from the transient infrared data matrices for (a) 7HQ stock solution (0 M $HCOO^-Cs^+$) and (b) 7HQ + 4.0 M $HCOO^-Cs^+$.

We compare the 2D SVD maps of the two (three) components with the sum of these components and the original data in Figure 13. The relevant components are shown in Figure 14, with fitting curves according to the following model.

We have used the following equations to describe the reaction kinetics. For the stock solution, we assume for the population decay of 7HQ-N*$_{FREE}$:

$$A(t) = e^{-t/\tau_1} \quad (1)$$

and for the population rise of 7HQ-Z*$_{FREE}$:

$$B(t) = 1 - e^{-t/\tau_1} \quad (2)$$

and find a time constant of τ_1 = 353 ± 45 ps, in accordance with our previously reported results.[48] For our case of 7HQ with 4.0 M $HCOO^-Cs^+$ we have used the following equations. For the fraction of "tight" complexes, the amount of 7HQ-N* disappearing (and accordingly 7HQ-A* getting formed) is governed by

$$A(t) = e^{-t/\tau_0} \quad (3)$$

with τ_0 < 0.2. For the fact that we analyze our transient UV/IR pump−probe results for pulse delay times >0.5 ps we argue that the A*$_{TIGHT}$ fraction is formed well within our time resolution. For the decay of N*$_{LOOSE}$ (parallel with rise of A*$_{LOOSE}$ and HCOOD$_{LOOSE}$), we use

$$B(t) = r \times e^{-t/\tau_1} + (1 - r) \times e^{-t/\tau_2} \quad (4)$$

Finally, for the decay of HCOOD$_{LOOSE}$ (parallel with rise of Z*, generated through the proton relay mechanism), we use

$$C(t) = e^{-t/\tau_3} - e^{-t/\tau_1} \quad (5)$$

From our fits we derive the following values for the time constants: τ_1 = 0.9 ± 0.08 ps, τ_2 = 75 ± 6 ps, and τ_3 = 490 ± 43 ps. We mimic here the dynamics of A*$_{LOOSE}$ and A*$_{REMOTE}$, with A*$_{REMOTE}$ reacting with formate as A*$_{LOOSE}$ after diffusional reorganization dynamics, as being governed by biexponential decaying functions. The effect of having a ratio of A*$_{LOOSE}$ and A*$_{REMOTE}$ on the overall observed reaction kinetics is taken into account with the ratio r. These results, despite the rather contained number of possible reaction pathways and possible bimolecular reaction dynamics assumed to follow single exponential reaction kinetics, suggest that we have grasped the essentials in the reaction kinetics of

https://dx.doi.org/10.1021/acs.jpca.0c10191
J. Phys. Chem. A 2021, 125, 1845−1859

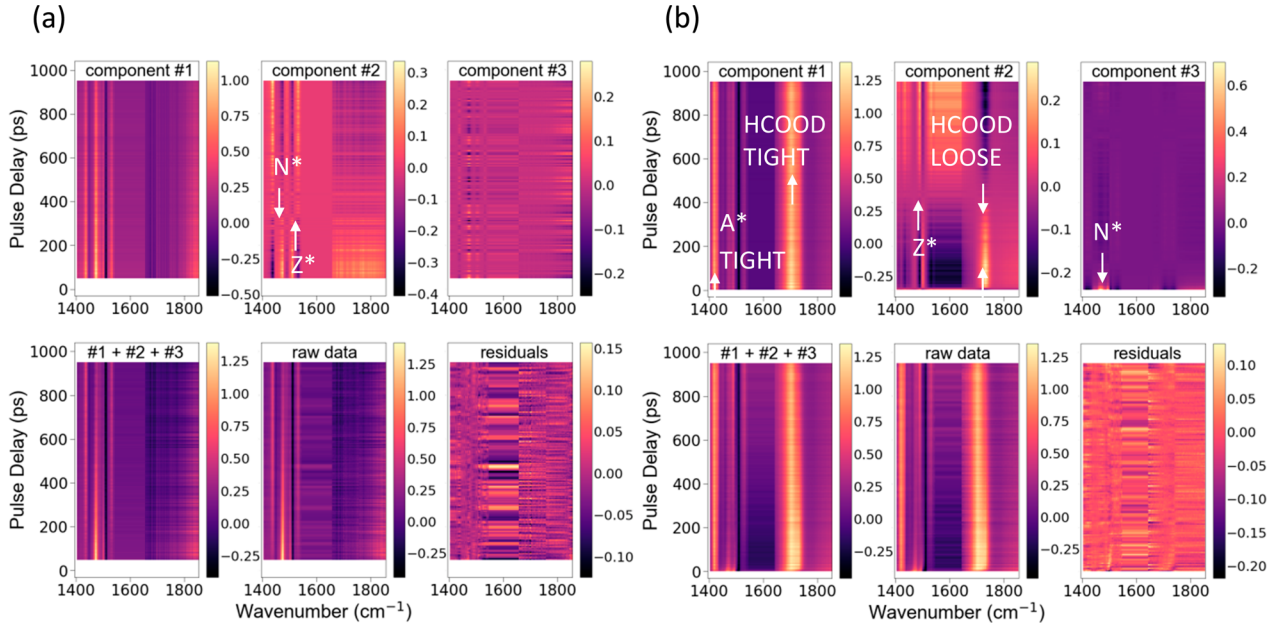

Figure 13. 2D SVD maps for (a) 7HQ stock solution (0 M $HCOO^{-}Cs^{+}$) and (b) 7HQ + 4.0 M $HCOO^{-}Cs^{+}$.

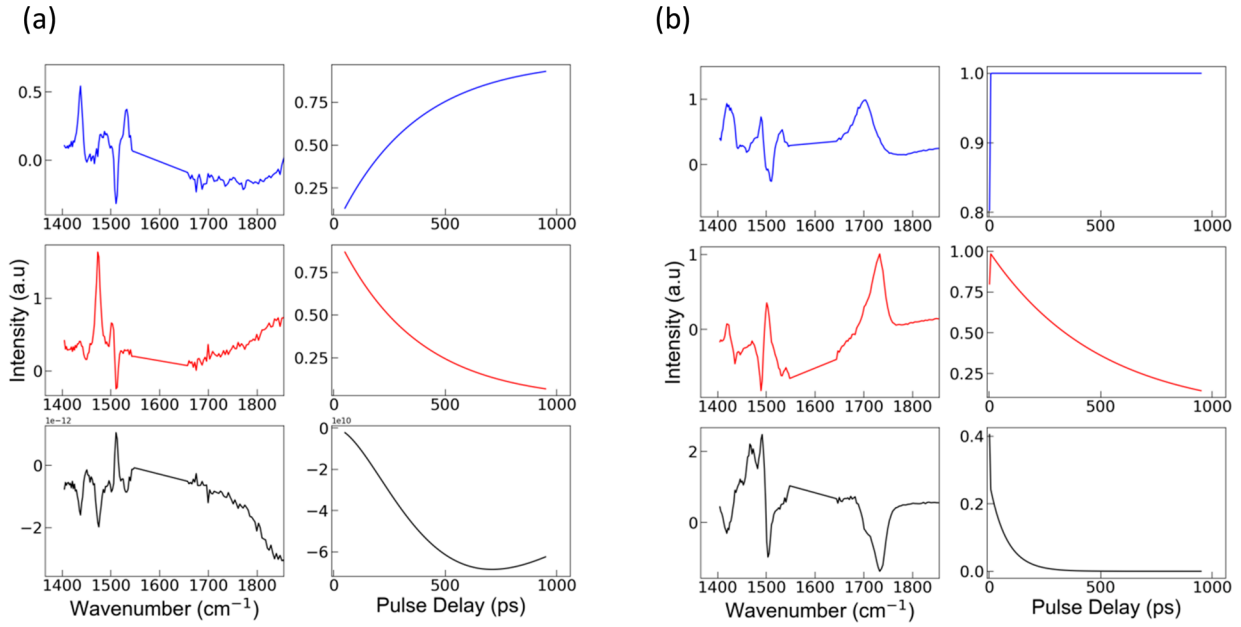

Figure 14. SVD components with corresponding fit curves for (a) 7HQ stock solution (0 M $HCOO^{-}Cs^{+}$) and (b) 7HQ + 4.0 M $HCOO^{-}Cs^{+}$.

photoexcited 7HQ and of the formate anion in CD_3OD. These will also apply for the measurements obtained with intermediate base concentrations of (0.5−4.0 M), albeit that a gradual shift in importance will occur from the contributions for the fraction of N^*_{FREE} toward those originating from N^*_{TIGHT} and N^*_{LOOSE}.

5. CONCLUSIONS

We have explored the photoinduced proton transfer reactions of 7-hydroxyquinoline (7HQ) in deuterated methanol in the presence of cesium formate. Whereas 7HQ in CD_3OD follows the N* → C* → Z* methanolysis pathway, where the rate-determining first step is the proton/deuteron abstraction by 7HQ-N* from the methanol solvent, adding $HCOO^{-}Cs^{+}$ at molar concentrations makes significant amounts of 7HQ-N* following the excess proton transfer pathway N* → A* → Z*. Major fractions of photoexcited 7HQ-N* exhibit the characteristics of "tight", i.e., "contact", and of "loose", i.e., "solvent-separated", acid−base reaction pairs. For the highest base concentrations, the remaining fraction of 7HQ-N* also follows this N* → A* → Z* pathway. A closer inspection of the temporal characteristics of 7HQ-N*, 7HQ-A*, 7HQ-Z*, and HCOOD, suggests that a fraction of HCOOD is involved as intermediate in the proton transport from the −OH group toward the quinoline N site of 7HQ. Future AIMD simulations may elucidate details on underlying microscopic mechanisms and the time ordering of the individual proton transfer steps, i.e., whether the solvent molecules being part of the proton transport bridge mediate proton transport via an excess proton or a proton vacancy mechanism. This could well be different

https://dx.doi.org/10.1021/acs.jpca.0c10191
J. Phys. Chem. A 2021, 125, 1845−1859

for a methanol solvent molecule located between the hydroxyl 7HQ-OH group and a formate anion or for a methanol molecule located between the quinoline N site of 7HQ and a transiently formed formic acid. Understanding the microscopic details of proton transport through solvent molecules in direct interaction with the negatively charged carboxylate ionic functionalities, as well as acids with hydroxyl or protonated amine functionalities, will be of help in the study of proton transport through transmembrane proteins and hydrogen fuel cells. For biological systems these involve, e.g., the side groups of serine, tyrosine, histidine, and asparagine amino acids forming the protein pockets around the proton channels, or for hydrogen fuel cells, the roles of ionic Coulomb fields of sulfonate anion or the particular superacids like sulfonic acids, as well as the organic amine bases like imidazole.

■ ASSOCIATED CONTENT

Supporting Information

The Supporting Information is available free of charge at https://pubs.acs.org/doi/10.1021/acs.jpca.0c10191.

Acidities and reactivities as estimated for 7HQ and formic acid in H_2O, CH_3OH, and CD_3OD solution, FT-IR spectra of formic acid in polar and nonpolar solvent mixtures (HCOOH in DMSO-d_6:CCl_4), average distances and angles and lifetimes of hydrogen bonds between 7HQ and the formate anion (PDF)

■ AUTHOR INFORMATION

Corresponding Authors

Daniel Sebastiani − *Institut für Chemie, Martin-Luther-Universität Halle-Wittenberg, 06120 Halle, Saale, Germany*; Email: daniel.sebastiani@chemie.uni-halle.de

Erik T. J. Nibbering − *Max Born Institut für Nichtlineare Optik und Kurzzeitspektroskopie, 12489 Berlin, Germany*; orcid.org/0000-0001-5874-8052; Email: nibberin@mbi-berlin.de

Authors

Marius-Andrei Codescu − *Max Born Institut für Nichtlineare Optik und Kurzzeitspektroskopie, 12489 Berlin, Germany*

Moritz Weiß − *Institut für Chemie, Martin-Luther-Universität Halle-Wittenberg, 06120 Halle, Saale, Germany*

Martin Brehm − *Institut für Chemie, Martin-Luther-Universität Halle-Wittenberg, 06120 Halle, Saale, Germany*

Oleg Kornilov − *Max Born Institut für Nichtlineare Optik und Kurzzeitspektroskopie, 12489 Berlin, Germany*; orcid.org/0000-0002-3343-2614

Complete contact information is available at: https://pubs.acs.org/10.1021/acs.jpca.0c10191

Notes

The authors declare no competing financial interest.

■ ACKNOWLEDGMENTS

This work has benefitted from financial support by the German Science Foundation (Deutsche Forschungsgemeinschaft (DFG) Project Number NI 492/13-1/SE 1008/11-1 (E.T.J.N. and D.S.) and Deutsche Forschungsgemeinschaft (DFG) Project Number BR 5494/1-1; M.B.) as well as the European Research Council (ERC) under the European Union's Horizon 2020 research and innovation programme (ERC Grant Agreement No. 788704; E.T.J.N.).

■ REFERENCES

(1) Horton, P.; Ruban, A. V.; Walters, R. G. Regulation of Light Harvesting in Green Plants. *Annu. Rev. Plant Physiol. Plant Mol. Biol.* **1996**, *47*, 655−684.

(2) Nelson, N.; Yocum, C. F. Structure and Function of Photosystems I and II. *Annu. Rev. Plant Biol.* **2006**, *57*, 521−565.

(3) Reece, S. Y.; Hamel, J. A.; Sung, K.; Jarvi, T. D.; Esswein, A. J.; Pijpers, J. J. H.; Nocera, D. G. Wireless Solar Water Splitting Using Silicon-Based Semiconductors and Earth-Abundant Catalysts. *Science* **2011**, *334*, 645−648.

(4) Scholes, G. D.; Fleming, G. R.; Olaya-Castro, A.; van Grondelle, R. Lessons from Nature About Solar Light Harvesting. *Nat. Chem.* **2011**, *3*, 763−774.

(5) Wang, J. L.; Wang, C.; Lin, W. B. Metal-Organic Frameworks for Light Harvesting and Photocatalysis. *ACS Catal.* **2012**, *2*, 2630−2640.

(6) Mauritz, K. A.; Moore, R. B. State of Understanding of Nafion. *Chem. Rev.* **2004**, *104*, 4535−4585.

(7) Kreuer, K.-D.; Paddison, S. J.; Spohr, E.; Schuster, M. Transport in Proton Conductors for Fuel-Cell Applications: Simulations, Elementary Reactions, and Phenomenology. *Chem. Rev.* **2004**, *104*, 4637−4678.

(8) Ramaswamy, P.; Wong, N. E.; Shimizu, G. K. H. Mofs as Proton Conductors - Challenges and Opportunities. *Chem. Soc. Rev.* **2014**, *43*, 5913−5932.

(9) Marx, D.; Tuckerman, M. E.; Hutter, J.; Parrinello, M. The Nature of the Hydrated Excess Proton in Water. *Nature* **1999**, *397*, 601−604.

(10) Vuilleumier, R.; Borgis, D. Transport and Spectroscopy of the Hydrated Proton: A Molecular Dynamics Study. *J. Chem. Phys.* **1999**, *111*, 4251−4266.

(11) Schmitt, U. W.; Voth, G. A. The Computer Simulation of Proton Transport in Water. *J. Chem. Phys.* **1999**, *111*, 9361−9381.

(12) Tuckerman, M. E.; Marx, D.; Parrinello, M. The Nature and Transport Mechanism of Hydrated Hydroxide Ions in Aqueous Solution. *Nature* **2002**, *417*, 925−929.

(13) Marx, D. Proton Transfer 200 Years after Von Grotthuss: Insights from Ab Initio Simulations. *ChemPhysChem* **2006**, *7*, 1848−1870.

(14) Voth, G. A. Computer Simulation of Proton Solvation and Transport in Aqueous and Biomolecular Systems. *Acc. Chem. Res.* **2006**, *39*, 143−150.

(15) Markovitch, O.; Chen, H.; Izvekov, S.; Paesani, F.; Voth, G. A.; Agmon, N. Special Pair Dance and Partner Selection: Elementary Steps in Proton Transport in Liquid Water. *J. Phys. Chem. B* **2008**, *112*, 9456−9466.

(16) Vilčiauskas, L.; Tuckerman, M. E.; Bester, G.; Paddison, S. J.; Kreuer, K.-D. The Mechanism of Proton Conduction in Phosphoric Acid. *Nat. Chem.* **2012**, *4*, 461−466.

(17) Chen, M.; Zheng, L.; Santra, B.; Ko, H.-Y.; DiStasio, R. A., Jr.; Klein, M. L.; Car, R.; Wu, X. Hydroxide Diffuses Slower Than Hydronium in Water Because Its Solvated Structure Inhibits Correlated Proton Transfer. *Nat. Chem.* **2018**, *10*, 413−419.

(18) de Grotthuss, C. J. T. Sur la Décomposition de l'Eau et des Corps Qu'elle Tient en Dissolution à l'Aide de l'Électricité Galvanique. *Ann. Chim.* **1806**, *LVIII*, 54−74.

(19) Danneel, H. Notiz über Ionengeschwindigkeiten. *Z. Elektrochem. Angew. Phys. Chem.* **1905**, *11*, 249−252.

(20) Marx, D.; Chandra, A.; Tuckerman, M. E. Aqueous Basic Solutions: Hydroxide Solvation, Structural Diffusion, and Comparison to the Hydrated Proton. *Chem. Rev.* **2010**, *110*, 2174−2216.

(21) Park, J. M.; Laio, A.; Iannuzzi, M.; Parrinello, M. Dissociation Mechanism of Acetic Acid in Water. *J. Am. Chem. Soc.* **2006**, *128*, 11318−11319.

(22) Hassanali, A.; Giberti, F.; Cuny, J.; Kühne, T. D.; Parrinello, M. Proton Transfer through the Water Gossamer. *Proc. Natl. Acad. Sci. U. S. A.* **2013**, *110*, 13723−13728.

(23) Tolbert, L. M.; Solntsev, K. M. Excited-State Proton Transfer: From Constrained Systems to "Super" Photoacids to Superfast Proton Transfer. *Acc. Chem. Res.* **2002**, *35*, 19−27.

(24) Pines, D.; Pines, E., Solvent Assisted Photoacidity. In *Hydrogen-Transfer Reactions*, Hynes, J. T.; Klinman, J. P., Limbach, H.-H., Schowen, R. L., Eds.; Wiley-VCH: Weinheim, 2007; Vol. *1* (Physical and Chemical Aspects I-III), pp 377−415.
(25) Pines, E.; Huppert, D.; Agmon, N. Geminate Recombination in Excited-State Proton Transfer Reactions: Numerical Solution of the Debye-Smoluchowski Equation with Backreaction and Comparison with Experimental Results. *J. Chem. Phys.* **1988**, *88*, 5620−5630.
(26) Agmon, N.; Pines, E.; Huppert, D. Geminate Recombination in Proton-Transfer Reactions. II. Comparison of Diffusional and Kinetic Schemes. *J. Chem. Phys.* **1988**, *88*, 5631−5638.
(27) Prémont-Schwarz, M.; Barak, T.; Pines, D.; Nibbering, E. T. J.; Pines, E. Ultrafast Excited-State Proton-Transfer Reaction of 1-Naphthol-3,6-Disulfonate and Several 5-Substituted 1-Naphthol Derivatives. *J. Phys. Chem. B* **2013**, *117*, 4594−4603.
(28) Simkovitch, R.; Pines, D.; Agmon, N.; Pines, E.; Huppert, D. Reversible Excited-State Proton Geminate Recombination: Revisited. *J. Phys. Chem. B* **2016**, *120*, 12615−12632.
(29) Driscoll, E. W.; Hunt, J. R.; Dawlaty, J. M. Photobasicity in Quinolines: Origin and Tunability Via the Substituents' Hammett Parameters. *J. Phys. Chem. Lett.* **2016**, *7*, 2093−2099.
(30) Driscoll, E. W.; Hunt, J. R.; Dawlaty, J. M. Proton Capture Dynamics in Quinoline Photobases: Substituent Effect and Involvement of Triplet States. *J. Phys. Chem. A* **2017**, *121*, 7099−7107.
(31) Xie, Y.; Ilic, S.; Skaro, S.; Maslak, V.; Glusac, K. D. Excited-State Hydroxide Ion Release from a Series of Acridinol Photobases. *J. Phys. Chem. A* **2017**, *121*, 448−457.
(32) Gajst, O.; da Silva, L. P.; da Silva, J.; Huppert, D. Enhanced Excited-State Proton Transfer Via a Mixed Water-Methanol Molecular Bridge of 1-Naphthol-5-Sulfonate in Methanol-Water Mixtures. *J. Phys. Chem. A* **2018**, *122*, 4704−4716.
(33) Hunt, J. R.; Dawlaty, J. M. Photodriven Deprotonation of Alcohols by a Quinoline Photobase. *J. Phys. Chem. A* **2018**, *122*, 7931−7940.
(34) Sheng, W.; Nairat, M.; Pawlaczyk, P. D.; Mroczka, E.; Farris, B.; Pines, E.; Geiger, J. H.; Borhan, B.; Dantus, M. Ultrafast Dynamics of a "Super" Photobase. *Angew. Chem., Int. Ed.* **2018**, *57*, 14742−14746.
(35) Genosar, L.; Cohen, B.; Huppert, D. Ultrafast Direct Photoacid-Base Reaction. *J. Phys. Chem. A* **2000**, *104*, 6689−6698.
(36) Pines, E.; Magnes, B. Z.; Lang, M. J.; Fleming, G. R. Direct Measurement of Intrinsic Proton Transfer Rates in Diffusion-Controlled Reactions. *Chem. Phys. Lett.* **1997**, *281*, 413−420.
(37) Rini, M.; Magnes, B.-Z.; Pines, E.; Nibbering, E. T. J. Real-Time Observation of Bimodal Proton Transfer in Acid-Base Pairs in Water. *Science* **2003**, *301*, 349−352.
(38) Mohammed, O. F.; Pines, D.; Dreyer, J.; Pines, E.; Nibbering, E. T. J. Sequential Proton Transfer through Water Bridges in Acid-Base Reactions. *Science* **2005**, *310*, 83−86.
(39) Mohammed, O. F.; Pines, D.; Nibbering, E. T. J.; Pines, E. Base-Induced Solvent Switches in Acid-Base Reactions. *Angew. Chem., Int. Ed.* **2007**, *46*, 1458−1469.
(40) Adamczyk, K.; Prémont-Schwarz, M.; Pines, D.; Pines, E.; Nibbering, E. T. J. Real-Time Observation of Carbonic Acid Formation in Aqueous Solution. *Science* **2009**, *326*, 1690−1694.
(41) Konijnenberg, J.; Ekelmans, G. B.; Huizer, A. H.; Varma, C. Mechanism and Solvent Dependence of the Solvent-Catalyzed Pseudo-Intramolecular Proton-Transfer of 7-Hydroxyquinoline in the 1st Electronically Excited Singlet State and in the Ground-State of Its Tautomer. *J. Chem. Soc., Faraday Trans. 2* **1989**, *85*, 39−51.
(42) Bardez, E. Excited-State Proton Transfer in Bifunctional Compounds. *Isr. J. Chem.* **1999**, *39*, 319−332.
(43) Kwon, O.-H.; Lee, Y.-S.; Yoo, B. K.; Jang, D. J. Excited-State Triple Proton Transfer of 7-Hydroxyquinoline Along a Hydrogen-Bonded Alcohol Chain: Vibrationally Assisted Proton Tunneling. *Angew. Chem., Int. Ed.* **2006**, *45*, 415−419.
(44) Kwon, O.-H.; Mohammed, O. F. Water-Wire Catalysis in Photoinduced Acid-Base Reactions. *Phys. Chem. Chem. Phys.* **2012**, *14*, 8974−8980.
(45) Bekçioğlu, G.; Allolio, C.; Ekimova, M.; Nibbering, E. T. J.; Sebastiani, D. Competition between Excited State Proton and Oh-Transport Via a Short Water Wire: Solvent Effects Open the Gate. *Phys. Chem. Chem. Phys.* **2014**, *16*, 13047−13051.
(46) Ditkovich, J.; Mukra, T.; Pines, D.; Huppert, D.; Pines, E. Bifunctional Photoacids: Remote Protonation Affecting Chemical Reactivity. *J. Phys. Chem. B* **2015**, *119*, 2690−2701.
(47) Hoffmann, F.; Ekimova, M.; Bekçioğlu-Neff, G.; Nibbering, E. T. J.; Sebastiani, D. Combined Experimental and Theoretical Study of the Transient IR Spectroscopy of 7-Hydroxyquinoline in the First Electronically Excited Singlet State. *J. Phys. Chem. A* **2016**, *120*, 9378−9389.
(48) Ekimova, M.; Hoffmann, F.; Bekçioğlu-Neff, G.; Rafferty, A.; Kornilov, O.; Nibbering, E. T. J.; Sebastiani, D. Ultrafast Proton Transport between a Hydroxy Acid and a Nitrogen Base Along Solvent Bridges Governed by the Hydroxide/Methoxide Transfer Mechanism. *J. Am. Chem. Soc.* **2019**, *141*, 14581−14592.
(49) Plimpton, S. Fast Parallel Algorithms for Short-Range Molecular-Dynamics. *J. Comput. Phys.* **1995**, *117*, 1−19.
(50) Martínez, L.; Andrade, R.; Birgin, E. G.; Martínez, J. M. Packmol: A Package for Building Initial Configurations for Molecular Dynamics Simulations. *J. Comput. Chem.* **2009**, *30*, 2157−2164.
(51) Jorgensen, W. L.; Maxwell, D. S.; Tirado-Rives, J. Development and Testing of the OPLS All-Atom Force Field on Conformational Energetics and Properties of Organic Liquids. *J. Am. Chem. Soc.* **1996**, *118*, 11225−11236.
(52) Golze, D.; Hutter, J.; Iannuzzi, M. Wetting of Water on Hexagonal Boron Nitride@Rh(111): A Qm/Mm Model Based on Atomic Charges Derived for Nano-Structured Substrates. *Phys. Chem. Chem. Phys.* **2015**, *17*, 14307−14316.
(53) Youngs, T. G. A.; Hardacre, C. Application of Static Charge Transfer within an Ionic-Liquid Force Field and Its Effect on Structure and Dynamics. *ChemPhysChem* **2008**, *9*, 1548−1558.
(54) Nosé, S. A Unified Formulation of the Constant Temperature Molecular-Dynamics Methods. *J. Chem. Phys.* **1984**, *81*, 511−519.
(55) Nosé, S.; Molecular-Dynamics, A. Method for Simulations in the Canonical Ensemble. *Mol. Phys.* **1984**, *52*, 255−268.
(56) Martyna, G. J.; Klein, M. L.; Tuckerman, M. Nosé-Hoover Chains - the Canonical Ensemble Via Continuous Dynamics. *J. Chem. Phys.* **1992**, *97*, 2635−2643.
(57) Brehm, M.; Kirchner, B. Travis - a Free Analyzer and Visualizer for Monte Carlo and Molecular Dynamics Trajectories. *J. Chem. Inf. Model.* **2011**, *51*, 2007−2023.
(58) Brehm, M.; Thomas, M.; Gehrke, S.; Kirchner, B. Travis-a Free Analyzer for Trajectories from Molecular Simulation. *J. Chem. Phys.* **2020**, *152*, 164105.
(59) Humphrey, W.; Dalke, A.; Schulten, K. VMD: Visual Molecular Dynamics. *J. Mol. Graphics* **1996**, *14*, 33−38.
(60) Stone, J. E. An Efficient Library for Parallel Ray Tracing and Animation. *Masters Thesis*. 1998.
(61) Fang, W.-H. Ab Initio Study of the Triple-Proton-Transfer Reactions of Ground and Excited States of 7-Hydroxyquinoline in Methanol Solution. *J. Am. Chem. Soc.* **1998**, *120*, 7568−7576.
(62) Park, S.-Y.; Kim, H.-B.; Yoo, B. K.; Jang, D.-J. Direct Observation of Conformation-Dependent Pathways in the Excited-State Proton Transfer of 7-Hydroxyquinoline in Bulk Alcohols. *J. Phys. Chem. B* **2012**, *116*, 14153−14158.
(63) Lee, S.-I.; Jang, D.-J. Proton Transfers of Aqueous 7-Hydroxyquinoline in the First Excited Singlet, Lowest Triplet, and Ground-States. *J. Phys. Chem.* **1995**, *99*, 7537−7541.
(64) Jazaj, D.; Ghadami, S. A.; Bemporad, F.; Chiti, F. Probing Conformational Changes of Monomeric Transthyretin with Second Derivative Fluorescence. *Sci. Rep.* **2019**, *9*, 10988.
(65) Munitz, N.; Avital, Y.; Pines, D.; Nibbering, E. T. J.; Pines, E. Cation-Enhanced Deprotonation of Water by a Strong Photobase. *Isr. J. Chem.* **2009**, *49*, 261−272.
(66) Rived, F.; Roses, M.; Bosch, E. Dissociation Constants of Neutral and Charged Acids in Methyl Alcohol. The Acid Strength Resolution. *Anal. Chim. Acta* **1998**, *374*, 309−324.

https://dx.doi.org/10.1021/acs.jpca.0c10191
J. Phys. Chem. A 2021, 125, 1845−1859

(67) Rived, F.; Canals, I.; Bosch, E.; Rosés, M. Acidity in Methanol-Water. *Anal. Chim. Acta* **2001**, *439*, 315−333.
(68) Cox, B. G. *Acids and Bases: Solvent Effects on Acid-Base Strengths*; Oxford University Press: Oxford, 2013.
(69) Pines, E.; Fleming, G. R. Proton-Transfer in Mixed Water Organic-Solvent Solutions - Correlation between Rate, Equilibrium-Constant, and the Proton Free-Energy of Transfer. *J. Phys. Chem.* **1991**, *95*, 10448−10457.
(70) Pines, E. The Kinetic Isotope Effect in the Photo-Dissociation Reaction of Excited-State Acids in Aqueous Solutions. In *Isotope Effects in Chemistry and Biology*; Kohen, A., Limbach, H.-H., Eds.; CRC Taylor & Francis: Boca Raton, 2006; pp 451−464.
(71) Mohammed, O. F.; Pines, D.; Pines, E.; Nibbering, E. T. J. Aqueous Bimolecular Proton Transfer in Acid-Base Neutralization. *Chem. Phys.* **2007**, *341*, 240−257.
(72) Spies, C.; Shomer, S.; Finkler, B.; Pines, D.; Pines, E.; Jung, G.; Huppert, D. Solvent Dependence of Excited-State Proton Transfer from Pyranine-Derived Photoacids. *Phys. Chem. Chem. Phys.* **2014**, *16*, 9104−9114.
(73) Maçôas, E. M. S.; Khriachtchev, L.; Pettersson, M.; Fausto, R.; Räsänen, M. Rotational Isomerism of Acetic Acid Isolated in Rare-Gas Matrices: Effect of Medium and Isotopic Substitution on Ir-Induced Isomerization Quantum Yield and Cis -> Trans Tunneling Rate. *J. Chem. Phys.* **2004**, *121*, 1331−1338.
(74) Marushkevich, K.; Khriachtchev, L.; Lundell, J.; Domanskaya, A. V.; Räsänen, M. Vibrational Spectroscopy of Trans and Cis Deuterated Formic Acid (HCOOD): Anharmonic Calculations and Experiments in Argon and Neon Matrices. *J. Mol. Spectrosc.* **2010**, *259*, 105−110.
(75) Giubertoni, G.; Meister, K.; DeVries, A. L.; Bakker, H. J. Determination of the Solution Structure of Antifreeze Glycoproteins Using Two-Dimensional Infrared Spectroscopy. *J. Phys. Chem. Lett.* **2019**, *10*, 352−357.
(76) Stepanian, S. G.; Adamowicz, L. The Effect of Matrices on the Low-Temperature Ir Spectra of a Formic Acid Molecule Isolated in Inert Gas Crystals. *Low Temp. Phys.* **2020**, *46*, 155.
(77) Bach, A.; Coussan, S.; Muller, A.; Leutwyler, S. Water-Chain Clusters: Vibronic Spectra of 7-Hydroxyquinoline • $(H_2O)_2$. *J. Chem. Phys.* **2000**, *112*, 1192−1203.
(78) Bach, A.; Coussan, S.; Muller, A.; Leutwyler, S. Water-Wire Clusters: Vibronic Spectra of 7-Hydroxyquinoline • $(H_2O)_3$. *J. Chem. Phys.* **2000**, *113*, 9032−9043.

https://dx.doi.org/10.1021/acs.jpca.0c10191
J. Phys. Chem. A 2021, 125, 1845−1859